DOI: 10.13009/EUCASS2019-439

An Investigation into Injector Architecture for Sub-Newton Monopropellant Propulsion

*Ewan Fonda-Marsland *, Graham Roberts *, Dave Gibbon **, Charlie Ryan **
** University of Southampton, Southampton, SO17 1BK, UK*
eafm1g15@soton.ac.uk, G.T.Roberts@soton.ac.uk, C.N.Ryan@soton.ac.uk
*** Surrey Satellite Technology Ltd., Tycho House, Guildford, GU2 7YE, UK*
D.Gibbon@SSTL.co.uk

Abstract

This paper presents an exploration of injector architecture candidates, including orifice and Poiseuille-type injectors, for sub-newton monopropellant thrusters. While the work here is specific to High Test Peroxide, it is expected to be applicable to other monopropellants. This methodology presented here seeks to underpin the fluid mechanics through flow characterisation and hot firing of each injector, with analytical, experimental and computational methods. Experimental results broadly follow calculations and simulations, although do not fully agree. Further work is required to fully understand the microscale fluid dynamics, especially as chugging may not be as significant for sub-newton scale monopropellant thrusters.

1. Introduction

The ongoing trend of satellite miniaturisation, especially in the commercial sector, as well as the continued interest of integrating propulsion system on CubeSat-scale spacecraft is driving the development of small propulsion systems [1, 2]. While electric propulsion has garnered recent interest for these applications, it typically comes with drawbacks, such as constant power requirements and low thrust to system volume ratios [2]. Novel liquid chemical monopropellant systems are contenders to these electric systems, especially given the advent of lower toxicity *green* propellants such as those based on hydroxyl-ammonium nitrate (HAN), ammonium dinitramide (ADN) and High Test Peroxide (HTP). Monopropellant systems are ideal candidates for providing low thrusts in small system volumes due to their low system complexity, requiring a single propellant delivery system and a thruster comprised of an injector, catalyst bed and nozzle.

For low thrust levels, especially in the sub-newton range, monopropellant thruster designs encounter some key challenges: the reduced propellant flow rates require very small geometry, posing difficulties for manufacture as well as physical phenomena not present or significant in larger systems. Problems arising from micro-nozzles, including the increased impact of viscous effects and incomplete flow development have been studied [3, 4], however, to date there have only been some limited investigations into characterising the underpinning design and performance issues of injectors for micro monopropellant propulsion.

Conventionally, injectors serve two main purposes: the control of the propellant flow rate into the thruster and the distribution of the propellant over the upstream of a catalyst bed [5, 6]. The former determines the performance of a propulsion system and decouples the turbulent decomposition regime in the chamber from the upstream propellant feed line, preventing pressure instabilities from developing. The latter is also important for the system performance as it maximises the usage of the catalyst bed, reducing the size of the bed, which is especially important for smaller thrusters as any extra thermal mass will result have a large impact on the chamber temperature.

There is a good understanding of injector design criteria for large scale monopropellant systems, however injectors for small monopropellant thrusters have much less documentation. While some research in literature has looked at specific injector implementations and how performance is affected by the different architectures of both the injector and thruster [6-14], the underpinning physical processes relating to the design of an injector of this scale hasn't been studied in depth. This paper presents a preliminary investigation into different design and characterisation approaches for injectors for sub-newton monopropellant systems, both in terms of experimental testing as well as analytical and computational methods. The research looks specifically at a 0.1 N nominal thrust propulsion system using 87.5% /wt. HTP, although the methodology is expected to be applicable to other systems. An example thruster of this scale with a nominal chamber pressure of 8 bar, has mass flow rates ranging between 0.150 $g.s^{-1}$ and 0.037 $g.s^{-1}$ for a 25 bar to 5 bar blowdown system, corresponding to a range of thrusts of 0.266 N and 0.07 N respectively.

DOI: 10.13009/EUCASS2019-439

2. Injector Architectures

2.1 Injector Purposes

Conventionally in a monopropellant thruster, the injector controls the mass flow of propellant from the delivery system and distributes it over a catalyst bed. A good design is essential to optimise performance over a typical lifetime blowdown range [11]. As mentioned, one key aspect of the flow control is to decouple the propellant feed line from the turbulent regime in the decomposition chamber, which can lead to periodic pressure instabilities known as *chugging* in the system, degrading performance. This decoupling is typically achieved by dropping pressure over the injector, effectively choking the flow and limiting the propagation of transient pressure fluctuations upstream into the feed line [6]. A drawback of this is that it trades performance for the improved stability as the chamber pressure must be reduced for a given system pressure. Careful optimisation must be considered to maximise the performance of a given propulsion system while reducing or eliminating the likelihood of these instabilities. Pressure drops considered 'safe' for HTP monopropellants, reducing the risk of chugging are often cited in the range of 5% to 20% of the chamber pressure [10-12].

Injectors also serve to distribute propellant over the entire cross-sectional area of the thruster, and macroscale designs with multiple inlets or ones which spray the fluid over a wide area are commonly used [6]. However, the length scales of 0.1 N thrust monopropellants are so small that macroscale methods are impractical. For example, for a 5% pressure drop at End-of-Life (EoL) of the example 0.1 N thruster, an ideal conventional injector would require a single orifice diameter of ~ 63.3 µm, and multiple ports would lower this even further. Additionally the current work considers determining the underpinning physical mechanisms a primary goal, and should be extendable to more complex designs.

2.2 Injector Architectures

Three types of geometry capable of injector architecture have been identified: an orifice injector, a thin plate with one or more holes; a Poiseuille injector, a long micro-bore tube; and a porous injector, a volume of permeable material. Each architecture uses a different method to create a pressure drop and are described by analytical equations relating the pressure drop dP, mass flow rate $\dot{m}$, fluid physiochemical properties, and the specific injector geometry. For an orifice injector a simplified form of the *Bernoulli principle* is used, the Poiseuille architecture uses the *Hagen-Poiseuille Law*, and *Darcy's Law* is used to describe the flow through a porous injector:

$$dP_{orifice} = \dot{m}^2 \frac{1}{2\rho} \frac{1}{C_d^2 A_{orifice}^2} = \dot{m}^2 \frac{1}{2\rho} \frac{1}{\zeta_{orifice}^2} \tag{1}$$

$$dP_{poiseuille} = \dot{m} \frac{8\pi\mu}{\rho} \frac{L_{inj}}{C_d A_{poiseuille}^2} = \dot{m} \frac{8\pi\mu}{\rho} \frac{1}{\zeta_{poiseuille}} \tag{2}$$

$$dP_{porous} = \dot{m} \frac{\mu}{\kappa\rho} \frac{L_{inj}}{C_d A_{porous}} = \dot{m} \frac{\mu}{\kappa\rho} \frac{1}{\zeta_{porous}} \tag{3}$$

Importantly, to preserve the general form between the equations, the geometric parameters have been grouped into a single variable ζ, such that $\zeta \propto \dot{m}/dP^i$. This term also includes an empirically derived coefficient of discharge C_d to describe non-ideal flow. This parameter is defined as $C_d = \dot{m}_{exp} / \dot{m}_{ideal}$ and as such should be below 1. This coefficient is independent of the working fluid and therefore the specific flow characteristics for any given injector must be determined.

The relationship between pressure drop and the geometric parameters is important as it highlights some key benefits and drawbacks of each type. Both orifice and Poiseuille injectors have $dP \propto 1/A^2$ so their performance is much more sensitive to variation in the cross-sectional size and shape than porous injectors – both important in both design and manufacturing. Additionally, both the Poiseuille and porous pressure drops are proportional to the injector length giving an extra design parameter, but as they both use viscous effects to control the flow, they are likely to be affected by surface finish and roughness.

Most flight monopropellant systems utilise a simple blow-down pressurisation system and therefore the injector will see a decreasing upstream pressure and mass flow rate over the lifetime of the system. For the Poiseuille and porous architectures $dP \propto \dot{m}$, so the pressure drop should be constant for a given chamber pressure. However orifice injects have $dP \propto \dot{m}^2$, so at the lower flow rates towards the EoL the pressure drop will be a smaller fraction of the chamber pressure. This is expected to increase the likelihood of coupled pressure instabilities. It is therefore especially important to determine the particular cause of the coupling and a method to select lower bounds for the pressure drop.

Note that while all three types of injector architecture should provide a suitable method to control the flow into a monopropellant thruster, the work from this point forward has only considered orifice and Poiseuille injector architectures. Future work will investigate porous injector types.

DOI: 10.13009/EUCASS2019-439

2.3 Injector Manufacturing Methods

Both the orifice and Poiseuille injector architectures were manufactured or procured using different methods. Table 1 lists the techniques used in the current work, however it is worth noting that only the chemical etching (orifice) and commercially procured cold-drawn (Poiseuille) articles were successful in producing repeatable working test articles. While this paper is not intended to be a manufacturing study, it is important to briefly discuss some details of the methodology for manufacture and procurement.

In the case of the orifice injectors, stainless steel 316L alloy material, 0.2 mm or thinner, was used. The conventional micro-machining has been successfully demonstrated for 1 N scale thrusters [11], however it was not considered feasible for this project given the small scales of the orifices. 0.2 mm thick sheet material was used for the laser drilled component, however this technique resulted in sputter on the injector surface that caused blockages are the start of testing. The process could be improved and would likely result in high quality injectors but the etching technique proved more reliable and lower cost. Etching was carried out on 0.05 mm thick sheet material, and demonstrated good repeatability, although there were some issues with the geometric accuracy of the orifices, discussed below. This method utilised an acid etchant, and geometry was controlled by a photosensitive resistive layer, with detailing exposed onto the resist using laser light.

For the Poiseuille injectors, it was established that techniques employed in other similar research [10, 12] using MEMS manufacturing were not easily adapted to a conventional axisymmetric monopropellant thruster. Cold-drawn stainless steel 304 alloy micro-bore tubing is readily available from commercial suppliers, as it is commonly used in gas chromatography. This injector type has proved effective, although there are some questions on the accuracy of the internal geometry of the components, as discussed later.

Table 1 – A list of injector architectures and manufacturing methods used in this paper.

Injector Architecture	Manufacturing Technique	Material	Minimum Length Scale [mm]	Source	Manufacturing Method Result	Manufactured Article Number
Orifice	Conventional Micro-machining	SS316L	0.15	Manufactured	Successful	3
Orifice	Laser Drilling	SS316L	0.036	Manufactured	Unsuccessful	1
Orifice	Chemical Etching	SS316L	0.05	Manufactured	Successful	17
Poiseuille	Cold-drawn Micro-bore Tubing	SS304	0.127	Procured	Successful	38

3. Steady-State Flow Characterisation

The analytical expressions in equations (1)-(3) provide a good preliminary estimation of the expected pressure drop for a given injector architecture and propellant mass flow rate, although they each have empirically derived coefficients which depend on a variety of physical parameters, including surface roughness, corner sharpness, and specific geometry. These can be determined by measuring flow of a working fluid, typically deionised (DI) water, through a given specimen over a range of mass flow rates, plotting the data such that a fitted characterisation curve corresponds to $dP_{inj}^{n}/\dot{m}$. This can be used to calculate a value for ζ, which describes the effective geometry and discharge characteristics for a specific injector, independent of the fluid.

Experimental measurements are made using a Coriolis mass flow meter and pressure transducer upstream of the injector inlet, measuring the mass flow rate, density and pressure of the working fluid prior to the injector. The fluid then passes through the injector to ambient atmospheric conditions. The pressure drop is assumed to be the difference between the upstream and ambient pressure, implying that the fluid has reached ambient environmental conditions before or at the injector exit plane.

An example of an orifice characterisation test is shown in Figure 1, including the raw data from the time domain as well as the extracted steady state characterisation data. This latter dataset has been fitted with a linear model, i.e. constant ζ. Note that the Poiseuille architecture characterisations are plotted on different axes to preserve linearity of lines of constant ζ.

DOI: 10.13009/EUCASS2019-439

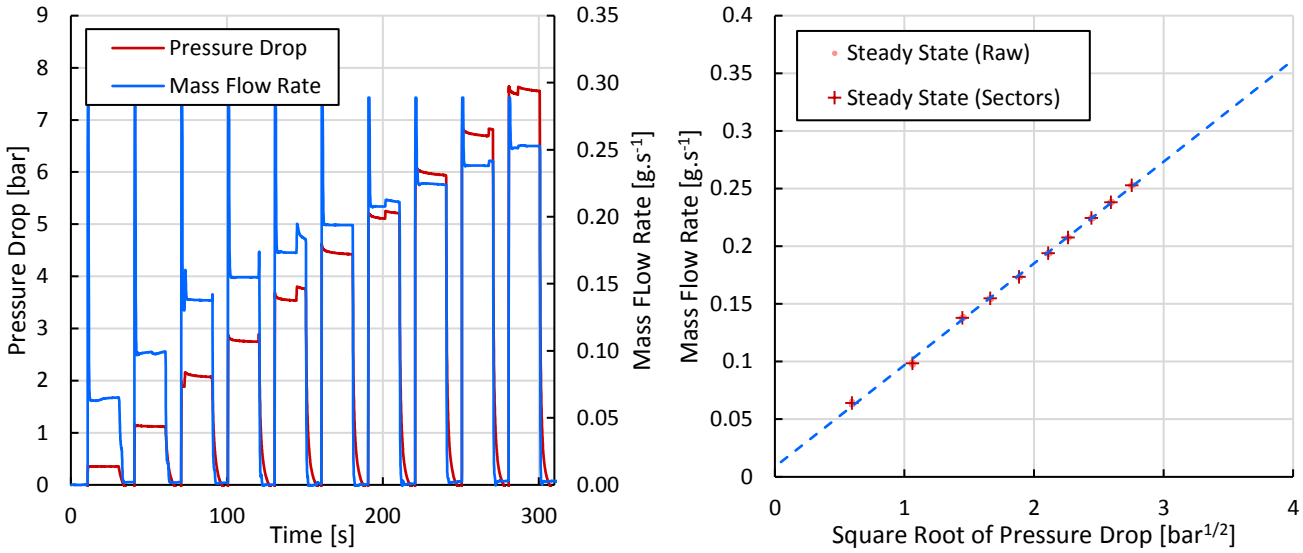

Figure 1: Example experimental flow characterisation test data (left) and steady state data (right) for an orifice injector. The steady state data has a linear fit model, indicating a constant ζ.

While this characterisation data can be used to estimate the performance of an injector with a downstream catalyst bed, it does not allow for an investigation into the microscale flow. This is difficult to do experimentally, so a computational model was developed, using the COMSOL Multiphysics commercial modelling software, to explore the underpinning dynamics. The model uses time-dependant multiphase laminar flow equations on an axisymmetric coordinate system. This simplifies the computations, and is expected to give a relatively close approximation of the flow given that the Reynolds number for a 50 µm orifice should be of the order of $R_e \sim 1500$, using a simplified version of Bernoulli's equation: $u_{inj,out} = \sqrt{2dP/rho}$. The flow is expected to be laminar, although this assumption is made based on macroscale fluid dynamics, which may not hold for smaller scales.

An example of the geometry and mesh for an orifice injector is shown in Figure 2. Note that the injector corners have been filleted with a high mesh density for stability and accuracy of the computation in these regions. Large fluid regimes have been included up and downstream of the injector to allow for the flow effects to fully propagate.

Initially a replication of the injector characterisation method, the intention of this model is to eventually apply it to variable downstream pressures to determine the specific conditions for the onset of chugging. However, in its current form, besides validating the model, it can also provide some insight into the steady state injector performance.

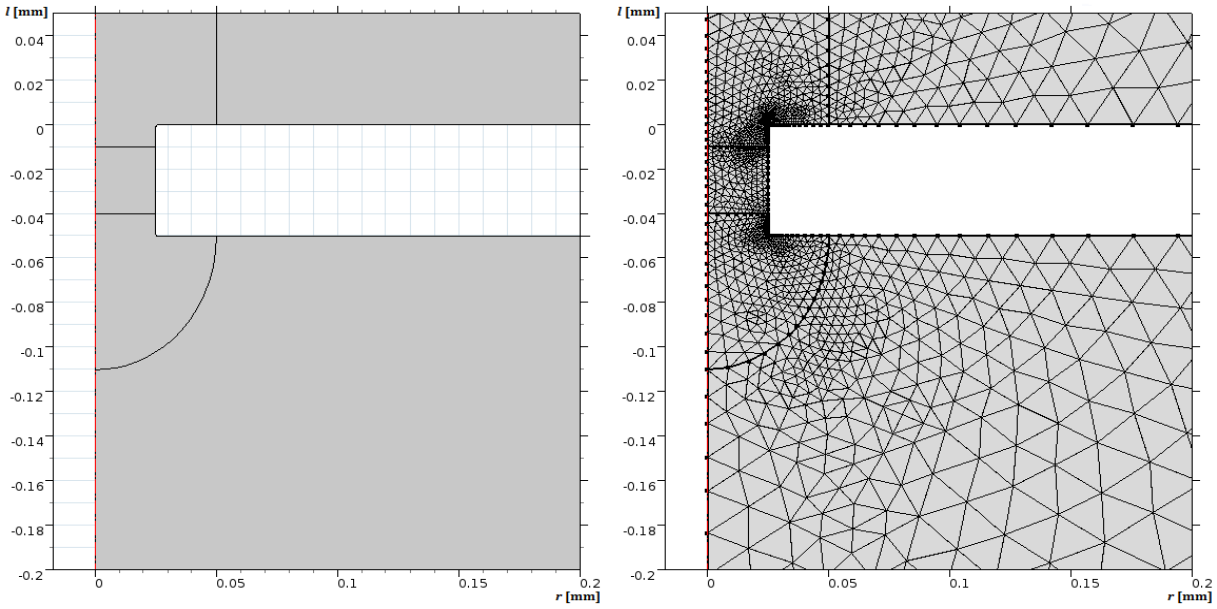

Figure 2: An example of the geometry and mesh for an axisymmetric injector. Note that the upstream (lower) portion of the mesh is only roughly refined due to reduced effects at a distance from the inlet.

DOI: 10.13009/EUCASS2019-439

3.1 Orifice Injector Characterisation

Table 2 includes a list of the injectors that were successfully manufactured using chemical etching, along with the designed and actual geometry of each. The actual area and effective diameter have been measured using optical microscopy, and it is worth noting that the areas given in the table are smaller than as designed. This is due to non-vertical wall profiles resulting from the etching process, illustrated in the example micrograph in Figure 3. In this image of one of the type 1-120-50 injectors, the area and effective diameter of the hole at the surface are calculated as 1.023×10^5 µm^2 and 118.0 µm, compared with 7.819×10^3 µm^2 and 99.78 µm for the inner orifice.

The inner orifice will be acting as the main flow restriction, and the analytical equation (1) assumes a thin plate, therefore this area is taken to be the *discharge* area used for further analysis. While this geometry misspecification is an issue for further manufacture using etching, it was not expected to cause significant issues in testing.

Table 2 – A list of orifice injector geometries, manufactured using chemical etching, including the optically measured.

Injector ID	Test Article Count	Design Orifice Diameter [µm]	Sheet Thickness [µm]	Orifice Number	Mean Total Discharge Area [m^2]	Mean Effective Discharge Orifice Diameter [µm]
1-50-50	3	50	50	1	312.3	19.94
1-80-50	3	80	50	1	1261	40.07
1-100-50	3	100	50	1	5581	86.53
1-120-50	2	120	50	1	7377	96.92
3-60-50	3	60	50	3	5801	85.94
5-50-50	3	50	50	5	10850	117.5

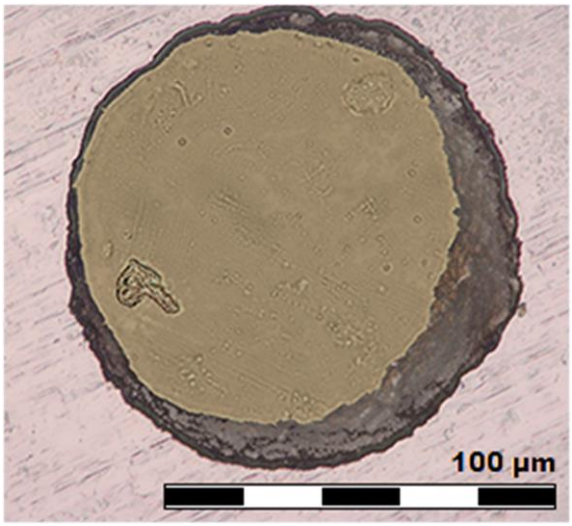

Figure 3: Example micrograph of etched orifice injector 1-120-50_1. Note that this is a combined image of reflection and transmission micrographs, generated using *extended focused image* for increase depth of field.

The results the experimental results are given in Table 3, note that some of the smaller orifice injectors blocked during testing or did not register sufficient mass flow rate to characterise accurately. In all of the successful tests, the gradient of $\dot{m}$ vs $\sqrt{dP}$ was linear, as expected from the analytical expression. However, the calculated discharge coefficients using the discharge area are all considerably larger than the expected upper bound of 1. It is currently unclear as to why this is the case, although it may be due to the wall profile of the orifice affecting the flow into the injector as the specific geometry isn't sharp-cornered and parallel to the axis. The pressure drop in an orifice injector is a result of the acceleration of the flow, and for sudden changes in area, flow acceleration is quite extreme. It has been suggested that the pressure drops below the vapour pressure of the working fluid causing localised cavitation [15, 16]. Further work looking at the specific geometry of the orifices, including more detailed 3D inspection, and analysis of the impact on the performance is required.

DOI: 10.13009/EUCASS2019-439

Table 3 – Results of the orifice injector characterisation test campaign.

Injector ID	Tested Article Count	Geometric Parameter [m]	Coefficient of Discharge	Standard Deviation of C_d
1-50-50	1 *	1.66×10^{-9}	2.72	
1-80-50	2 *	5.65×10^{-9}	3.44	0.71
1-100-50	3	1.34×10^{-8}	2.29	0.16
1-120-50	2	1.58×10^{-8}	2.15	0.10

* Some injectors either blocked or excessively flow rates precluding characterisation.

Preliminary simulations of a range of orifice injectors were carried out assuming a sharp-edged (small radius) orifices with a thickness of 50 µm and diameters corresponding to the discharge diameters from inspection. Table 4 lists the selected designs and results from each set of simulations. Each characterisation data point is fitted to two separate time-dependent simulations, run until steady state convergence, at 5 separate pressure drops between 0.025 bar and 4 bar. The coefficients of discharge are below 1 as expected, unlike the experimentally calculated values. The trend of C_d vs A of both datasets are similar, with a decreasing coefficient for a larger area. This is shown by the example in Figure 4, and may be due to the increasing effect of inertial forces relative to viscous forces. Considering the Reynolds number, as it is proportional to the characteristic flow velocity, as the injector discharge area decreases, both the fluid velocity and the Reynolds number will increase, so viscous forces will have less effect. Additionally this is potentially compounded with the reduced local pressure drop associated with the flow acceleration, resulting in a smaller cavitation bubble and greater viscous interaction between the fluid and the wall. This correlation between the orifice and cavitation bubble size is indicated in the surface plots in Figure 5, where the static pressure colour map has been clipped in regions where it falls below the vapour pressure, predicting the formation and size of a bubble.

Table 4 – Parameters and results of the orifice injector characterisation simulations.

Injector ID	Discharge Diameter [mm]	Geometric Parameter [m]	Coefficient of Discharge
1-50-50	0.05	1.61×10^{-9}	0.82
1-80-50	0.08	3.75×10^{-9}	0.75
1-100-50	0.10	5.49×10^{-9}	0.70

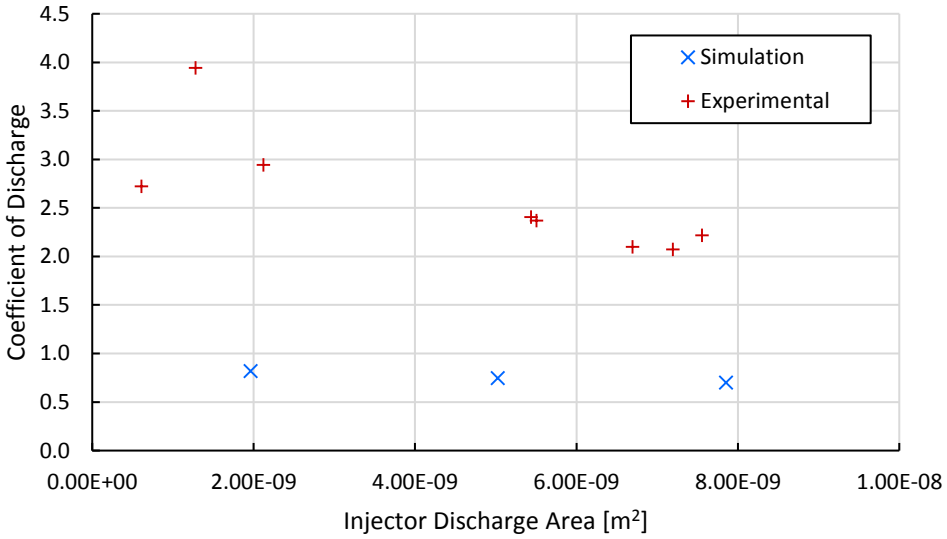

Figure 4: A comparison of orifice characterisation data for injector types 1-80-50 (experimental) and 1-50-50 (simulated) respectively, with discharge diameters of 51.99 µm and 50 µm respectively.

DOI: 10.13009/EUCASS2019-439

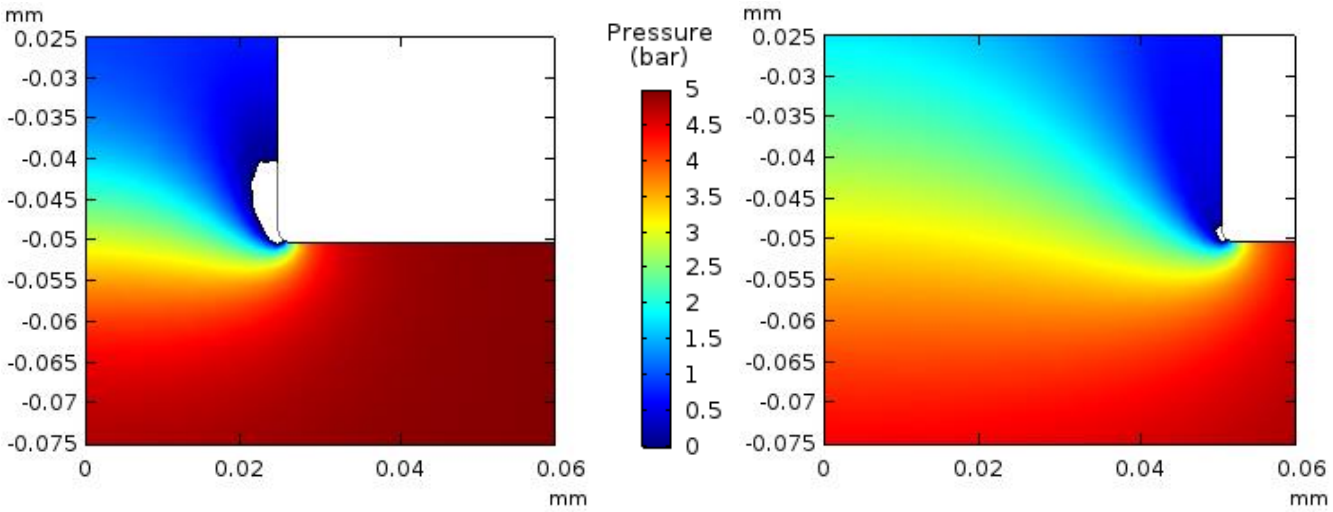

Figure 5: Example surface plots of the simulated static pressure of the flow through 100 µmØ (left) and 50 µmØ (right) orifice injectors focusing on the inlet corner. The colour represents the static pressure, with white clipping where the pressure is at or below the working fluid (DI) vapour pressure.

3.2 Poiseuille Injector Characterisation

A list of the different Poiseuille geometries procured for testing is given in Table 5. The cold-drawing manufacturing method used to make the steel microbore tubing results in rough internal geometry, shown in the x-ray computed tomography (CT) slice in Figure 6. It is difficult to inspect each tube to determine each mean diameter due to x-ray refraction and issues with accurately creating calibration samples, so the cross-sectional area of each injector is taken to be the specified design area. This means that any manufacturing defects are included in the coefficient of discharge, but it is assumed that there will be little difference in the manufacturing process between samples, the impact is expected to be minor.

Table 5 – A list of Poiseuille injector geometries, procured for testing.

Injector ID	Test Article Count	Design Micro-Bore Diameter [mm]	Tube Length [mm]
5-50	3	0.127	50
7-50	5	0.178	50
10-50	3	0.254	50
30-50	3	0.762	50
5-100	3	0.127	100
7-100	3	0.178	100
10-100	5	0.254	100
7-200	3	0.178	200
10-200	4	0.254	200
20-200	3	0.508	200
30-200	3	0.762	200

Traditionally these effects are considered to be related to frictional and turbulent forces as a result of surface roughness [17, 18], although neither of these are included as part of the simulation series discussed below. Several other mechanisms for microfluidic effects resulting in differences between the Hagen-Poiseuille equation and experimental data have been proposed in literature, including electro-viscous effects [19] (not considered in the modelling), slip boundary conditions [20] (also not considered in the computational modelling), and entrance effects [21]. None of these provide particularly satisfying explanations of the causes, and a more in-depth look is required, especially as this phenomenon is seen in the simplified laminar computational model. One potential cause proposed here are increased effects due to surface tension at the exit at the lower flow rates, as the inertial forces relative to tension forces should be decreased for lower exit velocities. This will be explored in greater depth in future research.

DOI: 10.13009/EUCASS2019-439

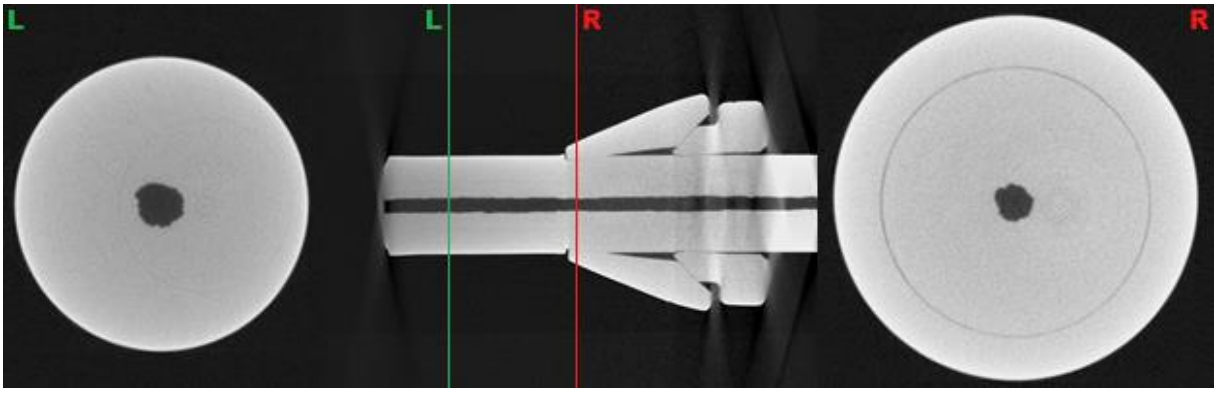

Figure 6: A slice of an example x-ray CT scan of part of a Poiseuille injector, showing the rough internal surface. This is one end of a type 10-100 injector with a compression fitting attached.

It is important to note that the nonlinearities are small, with the mean R^2 values of 0.9911 and 0.9970 for the straight and curved models respectively. While this is likely to have a significant effect on the reliability of the analytical equation over a wide range of pressures, given the constraints imposed by the mass flow rate range of the 0.1 N thruster and propellant delivery system, the linear model can be used for further calculations.

Unlike with the orifice injectors, the analytical equation (2) expects that $\zeta \propto \dot{m}/dP$, however all of the flow characterisations exhibit some nonlinearity. An example of this is given in Figure 7. It is attributed to the different method of operation between the Poiseuille and orifice injectors: as the micro-bore tubes use viscous forces acting along the length of the injector, rather than the Bernoulli Effect and potentially localised cavitation for an orifice.

Table 6 contains a list of the mean characterisation results for each injector design, including ζ and the linear C_d parameter. Note that there is a quite a large spread for some of the data points, with the standard deviation of the discharge coefficient up to 38% of the mean value. This suggests that there is some variation between each specific article, potentially stemming from manufacturing inconsistencies, however this has yet to be corroborated with inspection.

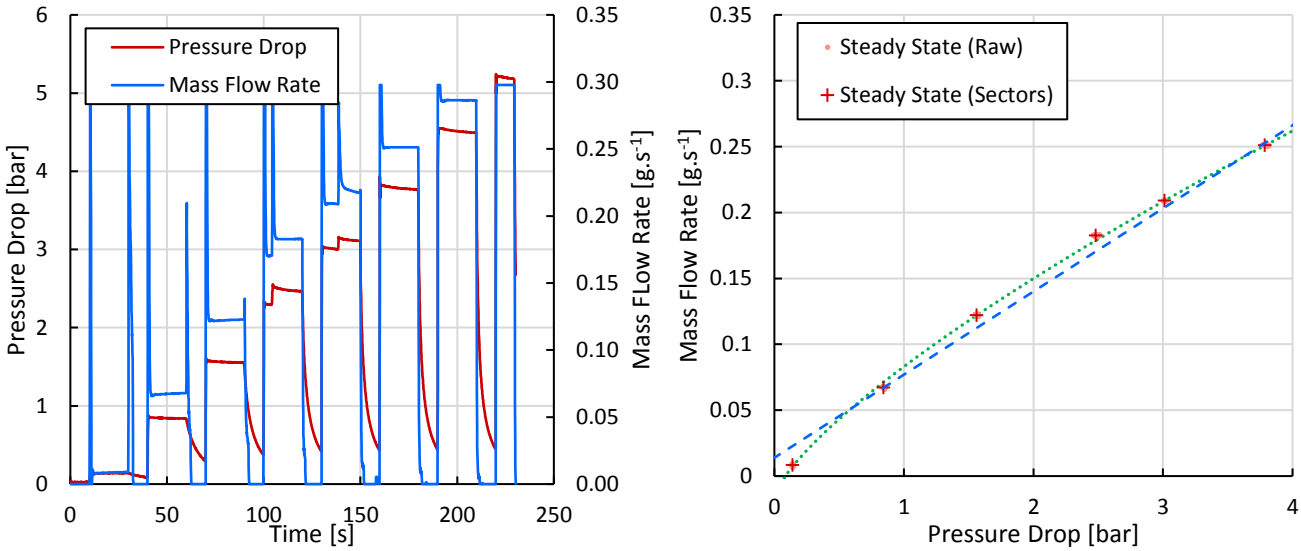

Figure 7: An example of the non-linearity of ζ in the experimental characterisation data for an injector of type 7-50, indicated by fitting both linear and power ($f(x) = ax^b + c$) models.

DOI: 10.13009/EUCASS2019-439

Table 6 - Results of the Poiseuille injector characterisation test campaign

Injector ID	Tested Article Count	Geometric Parameter [m]	Coefficient of Discharge	Standard Deviation of C_d
5-50	3	2.58×10^{-15}	0.80	0.31
7-50	5	7.84×10^{-15}	0.64	0.06
10-50	3	2.86×10^{-14}	0.56	0.02
30-50	0 *			
5-100	3	1.47×10^{-15}	0.92	0.04
7-100	3	5.17×10^{-15}	0.84	0.05
10-100	5	2.10×10^{-14}	0.82	0.17
7-200	3	2.90×10^{-15}	0.94	0.14
10-200	4	1.29×10^{-14}	1.01	0.28
20-200	0 *			
30-200	0 *			

* No characterisation data recorded due to excessively high or low flow rates.

A series of simulated flow characterisation for Poiseuille injector geometries given in Table 7 along with the characterisation results of each set of simulations. Each of these data points is generated from two separate time-dependent simulations, run until steady state convergence, at 5 separate pressure drops between 0.025 bar and 4 bar. While the results are of the same order of magnitude, they do not consistently match the experimental data: included in the table are the number of experimental standard deviations the simulation data falls from the mean experimental data. While this may be a result of manufacturing defects, it is clear that there are differences between the experimental and simulation results.

Figure 8 shows an example of both the experimental and simulation data for the characterisation of the type 10-100 injector geometry. While both exhibit the non-linearity discussed, the gradient and therefore ζ for the simulation data do not match the experimental values. This implies that either the potential manufacturing issues, or that the current numerical model does not completely capture all of the physical phenomena in the injector, for example turbulence or surface roughness.

Table 7 – Parameters and results of the Poiseuille injector characterisation simulations.

Injector ID	Internal Diameter [mm]	Length [mm]	Geometric Parameter [m]	Coefficient of Discharge	Standard Deviations between Simulation and Experimental Mean
5-50	0.127	50	3.34×10^{-14}	0.65	0.32
7-50	0.178	50	2.23×10^{-14}	0.87	4.34
10-50	0.254	50	1.07×10^{-14}	0.87	3.79
7-100	0.178	100	3.07×10^{-15}	0.96	0.40
10-100	0.254	100	1.21×10^{-14}	0.94	0.23
10-200	0.254	200	5.92×10^{-15}	0.96	2.68

DOI: 10.13009/EUCASS2019-439

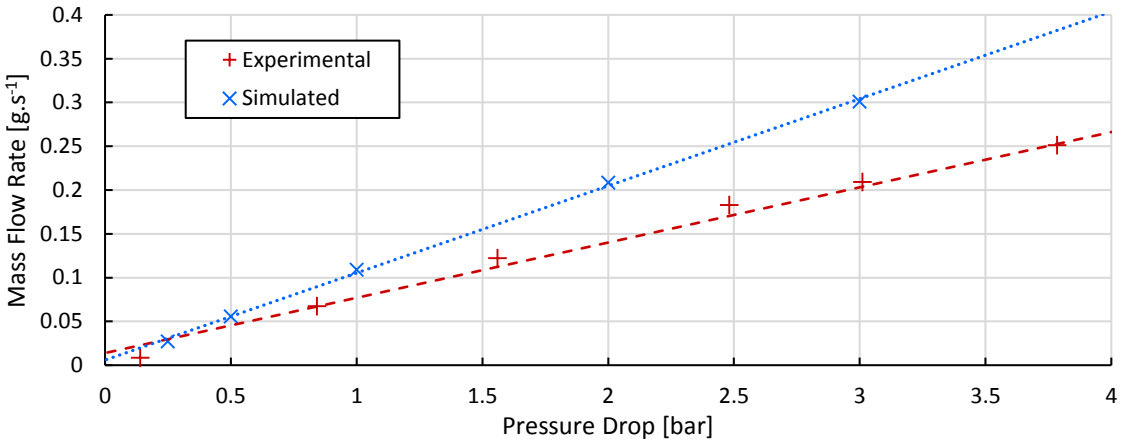

Figure 8: An example of the differences between experimental and simulated characterisation data set for the 10-100 type Poiseuille injector.

Contour maps of 3D second order polynomial models fit to the coefficient of discharge for both experimental and simulated data, as a function of the cross-section area and the reciprocal of the length, are given in Figure 9. Both exhibit broadly the same trend, with C_d increasing with length and decreasing with area. Both maps suggest that the coefficient of discharge is more sensitive to the length than the area. This implies that effects acting along the length, e.g. friction, impact the flow to a greater extent than the geometry of bore. However the increasing C_d with length is opposite to the expected trend: as the length increases flow impeding effects would be expected cumulatively, decreasing C_d. The large spread of experimental data could indicate that the assumption that the actual cross-sectional areas are similar for each design is wrong, however as it is also observed in simulations, it is likely a result of some fundamental physical effect requiring further investigation, and while there are some suggestions for potential causes, mentioned previously, there is no clear consensus as to its cause. It is important to state that much of the microfluidic literature suggests that the turbulent regime generally dominates at much lower Reynolds numbers than macroscale fluid systems [22, 23]

Worth noting is that despite the large spread of values for C_d as well as the currently unexplained trend in the value with respect to length, the geometric parameter ζ has been seen to give an accurate and repeatable estimation for the mass flow rate for a given pressure drop, and can be applied regardless of the working fluid. This makes it suitable for predicting the performance of an injector in a thruster.

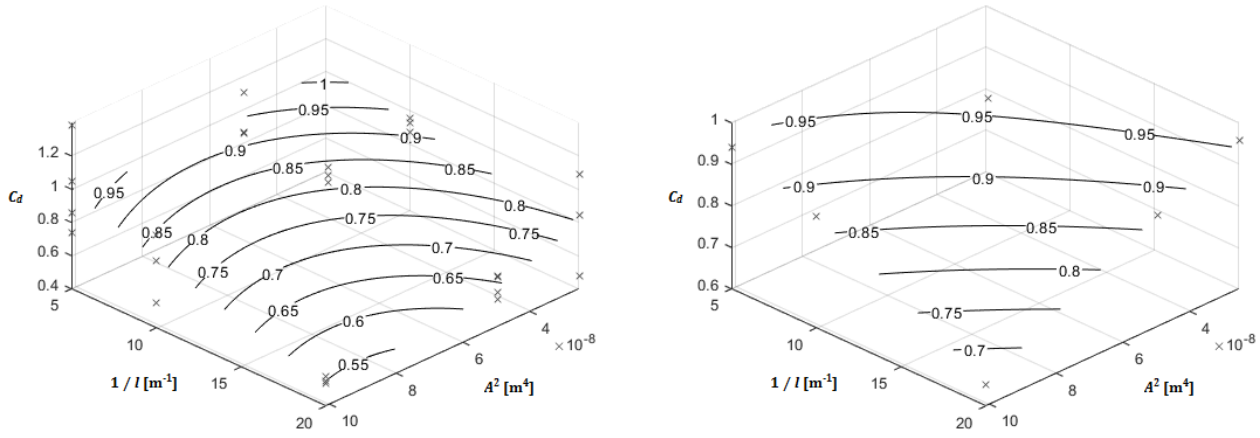

Figure 9: Contour maps of experimental (left) and simulated (right) Poiseuille discharge coefficients fitted with 3D second order polynomial function of the injector cross-sectional area and reciprocal of length. Recorded data points used to generate the fit are shown.

DOI: 10.13009/EUCASS2019-439

4. Injector Hot-Firing

Flow characterisation gives a good preliminary design metric to select an appropriate injector, however it is important to test a given injector with the propellant and a downstream catalyst bed. This is necessary as it not only validates the characterisation result, but *hot firing* of the thruster using a selection of different injectors over the operational pressure range will help determine the specific conditions resulting in chugging.

Several tests using both orifice and Poiseuille injectors were carried out using a 0.1 N breadboard 87.5% /wt. HTP thruster under ambient sea level conditions. The novel additive manufacturing (AM) of this thruster allows for multiple pressure taps along its length, notably before and after the injector. While the specific details of the thruster are less important for the analyses presented here, it has been designed with a nominal catalyst bed loading of 5.5 $kg.s^{-1}.m^{-2}$ at $P_{in} = 8$bar ($\dot{m} = 0.0624$ $g.s^{-1}$), and an L/D ratio of ~2. The resulting dimensions of the bed are 3.8 mmØ and 7.8 mm long. The catalyst is a commercially manufactured platinum active phase on 0.4 mmØ γ-alumina supports, retained at both ends by fine open-cell nickel foam discs. The propellant is injected directly onto the upstream retainer disc, which may also help to distribute the flow over the bed. A CAD drawing and photo showing the thruster are included in Figure 10.

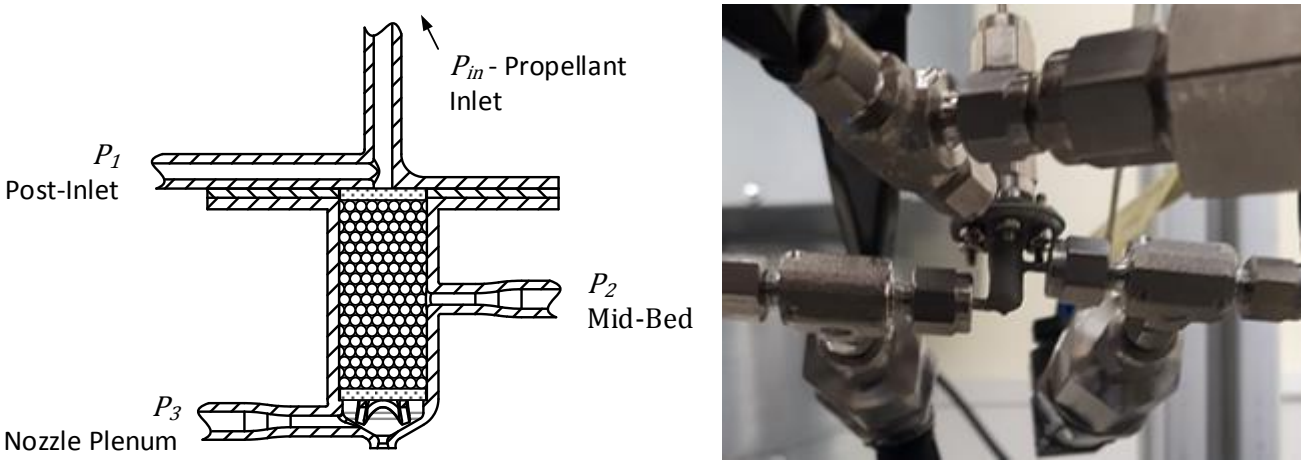

Figure 10: CAD (left) and photo (right) of the AM thruster with instrumentation standpipes indicated. The injector is not shown in the drawing, and the thruster in the photo has a Poiseuille injector attached.

Table 8 shows the test matrix, including the specific injector and range of inlet pressures successfully tested. Importantly the table also indicates the post-firing state of each injector. The Poiseuille injectors functioned well, however all of the orifice injectors blocked. This is a recurring issue with orifice injectors [11], and is attributed to the very small geometry. In this case of this test campaign the blockages most likely resulted from the sealing method of the breadboard thruster: the gasket binder appears to breakdown when exposed to HTP in the conditions close to the catalyst bed and some residue deposits in the orifice. Work is being done to resolve this issue, however it demonstrates that the Poiseuille architecture is more robust due to the larger geometry. While some steady state data was recorded for the orifice injectors, it is unclear whether this is for a fully functional or partially blocked injector.

Table 8 – Parameters and state of the injector hot-firing tests.

Injector ID	Test (Target) Inlet Pressures [bar]	Post-Firing State
1-80-50_2	5, 10	Blocked
1-80-50_3	5, 10, 20	Blocked
1-100-50_2	5, 10, 15	Blocked
SA-10-100_A	5, 10, 15, 20, 25	Functional
SA-10-50_B	5, 10, 15, 20, 25	Functional

4.1 Injector Flow Performance

Figure 11 shows an example plot of pressure and mass flow rate of a 60 s thruster firing with an inlet pressure of 10 bar dropped over the SA-10-100_A injector. Note that the mass flow rate drops as the inlet pressure blows down. The data are used to calculate the measured and the expected (from characterisation) pressure drop, with the mean results for all tests shown in the plots in Figure 12. Most of the experimental results of the orifice injectors show a

DOI: 10.13009/EUCASS2019-439

significantly higher pressure drop than expected from the flow characterisation modelling, confirming the blockage, while the Poiseuille datasets show relatively good agreement with the models.

Worth noting is that the smaller diameter SA-10-50_B injector has a systematically lower pressure drop than expected. This may be due to the observed non-linearity observed during characterisation, given that HTP has a higher dynamic viscosity than water, so any additional viscous losses related to the different working fluid should be less pronounced for a shorter injector. The injector temperature is also raised due to the proximity of the thruster, although this should only have a small effect as the maximum temperature at the injector plane (measured at the central axis) is only 86.1 °C and the rest of the injector is expected to be close to ambient.

An interesting effect, qualitatively observed with Poiseuille injectors that does not appear to affect orifice injectors, is a slower start-up transient. In all cases with microbore tubes, the pressure seems to propagate through the injector slower and the rise in P_c appears more gradual. This is difficult to quantitatively validate given the blockage issues with the orifice injectors, but the chamber pressure delay time $\tau_{90\%,P_c}$ appears to be approximately double for Poiseuille injectors for a specific P_{in}. While this needs confirming with more testing, there are certainly other implications besides pressure drop and distribution to selecting a specific injector architecture.

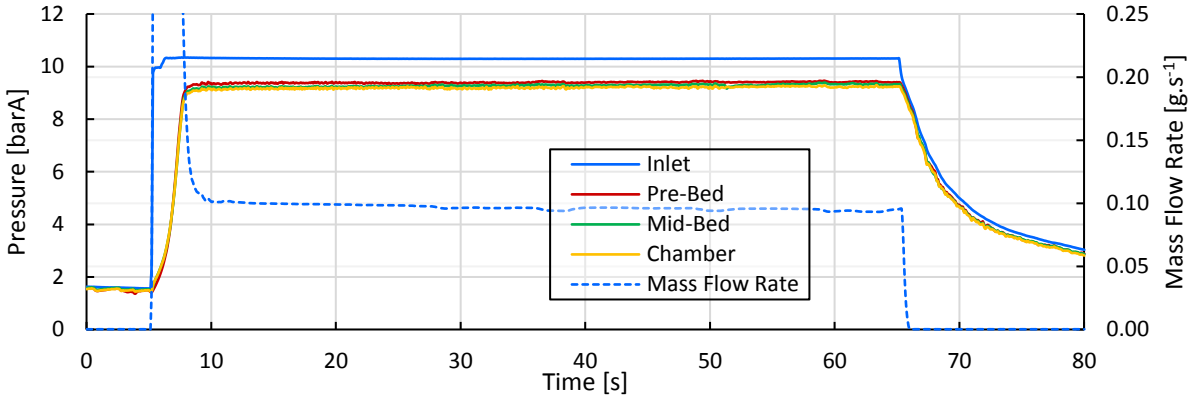

Figure 11: An example plot of the pressures and mass flow rates for a hot-firing run with a 0.1 N thruster. The test is with a target inlet pressure of 10 bar using injector SA-10-100_A.

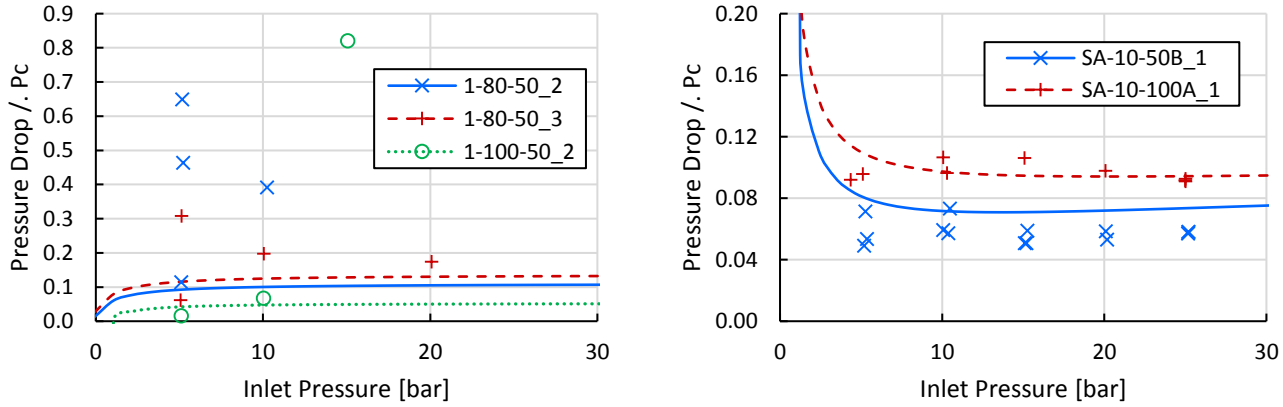

Figure 12: Pressure drop as a fraction of chamber pressure against inlet pressure for the orifice (left) and Poiseuille (right) injectors. The data is experimental (scatter) and modelled (curve - flow characterisation).

4.2 Pressure Coupling Performance

The different injector architectures may affect pressure instability coupling in different ways, with different critical pressure drops required to limit chugging. As this phenomenon is transient, frequency analysis of the pressure signals up and downstream of the injector is important. As discussed, the orifice injectors tested did not produce reliable data, so these analyses have been limited to the Poiseuille injector tests.

Pressure data was recorded upstream of the injector, at the injection plane, at the middle of the catalyst bed, and in the nozzle plenum. The data is linearly detrended to remove the effect of blowdown, normalised to zero, and run through a Fast Fourier Transform (FFT) algorithm to extract the frequency data. Figure 13 shows plots of the frequency spectra extracted from the steady state pressure data for all of the hot-firing runs with the SA-10-100_A injector. From these spectra, there appear to be two large frequency peaks that shift depending on the inlet pressure, from approximately 25 Hz @ $P_{in} = 5$ bar to ~100Hz @ $P_{in} = 25$ bar. This is likely related to the chugging pressure instabilities, which are typically expected of the magnitude of 10s of Hz [14, 24], and is expected to be a property of

DOI: 10.13009/EUCASS2019-439

the conditions, (e.g. pressure, mass flow rate, temperature etc.) as well as the specific geometry of the thruster and bed. Worth noting is that the exact frequency of these peaks also changes run-to-run for a given pressure, which is suggested to be a product of the specific packing of the catalyst. The magnitude of these particular modes also appears to increase with the inlet pressure, up to $P_{in} = 20$ bar, before decreasing.

It is apparent that that these oscillatory modes propagate throughout the thruster and up into the propellant feed line. However the maximum amplitudes appear at the injection plane, decreasing both through the thruster and injector. The catalyst bed is expected to damp out these oscillations as the packed catalyst pellets should provide some resistance to the flow, as expected with a porous injector. Unfortunately neither Poiseuille injectors appear to have fully decoupled the decomposition chamber from the feed line, however this does not have seem to have significantly affected the thruster performance.

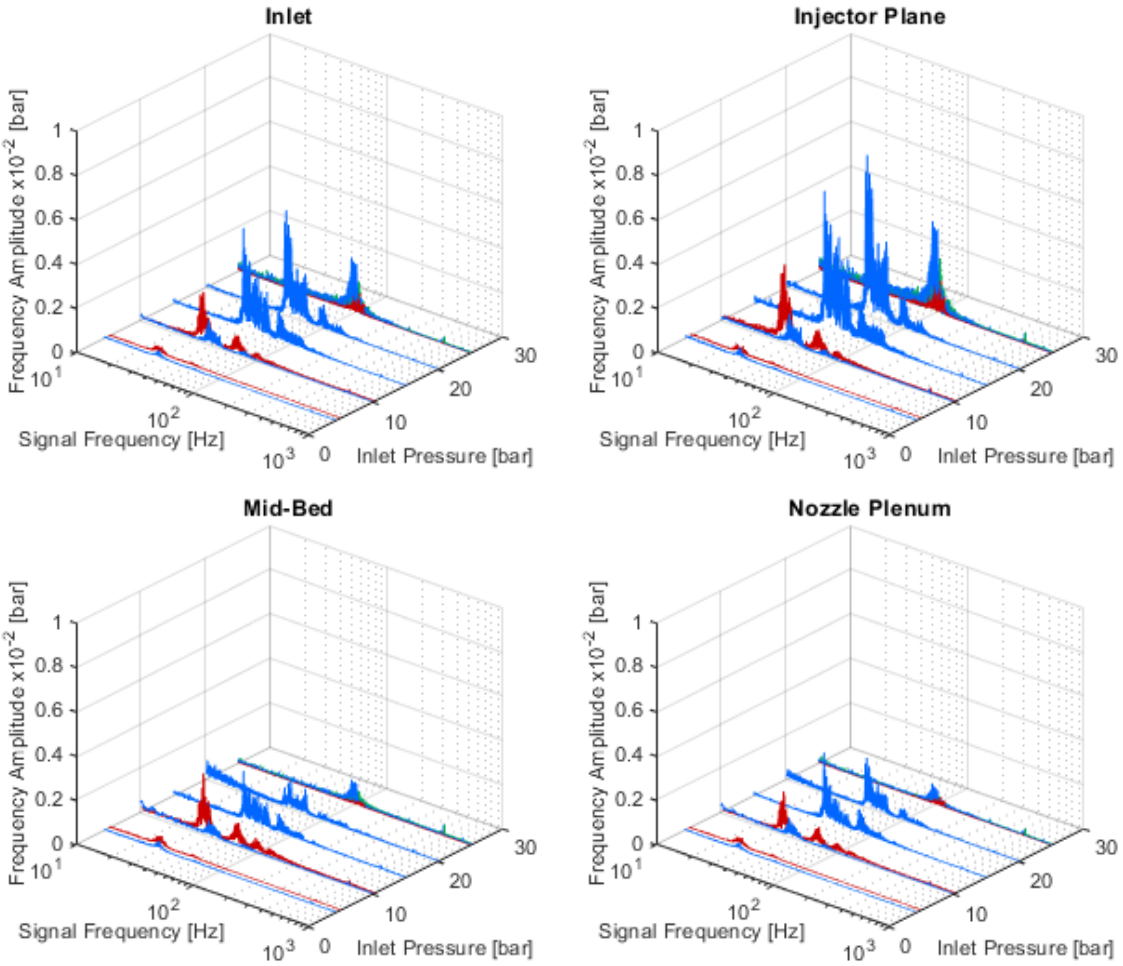

Figure 13: Example frequency spectra plots of the hot-firing datasets for the SA-10-100_A Poiseuille injector tests. Note that the lines have been coloured to help distinguish similar P_{in} overlapping runs.

As the frequency peaks do not line up, the data cannot be ensemble averaged and are instead compared for each run. Figure 14 shows a comparison of the peak amplitudes of the pressure signals across the injector. All of the results are 1 or below so both injectors are damping the pressure coupling, however due to the spread of data it is unclear as to whether the different lengths of the injector are significantly affecting this effect. Poiseuille injectors do not accelerate the flow to the same extent as orifice injectors and cavitation is not expected so the flow through a microbore tube is not expected to choke. This suggests that Poiseuille injectors will not decouple the pressure oscillations as effectively as orifice injectors, however more data is required to validate this. Additionally, a wider selection of lengths and discharge areas need to be considered to see if there is any significant effect on the decoupling.

The magnitudes of the oscillations are also important to consider. The amplitude for the largest peaks across all inlet pressures are 4.741 $\times 10^{-3}$ bar ($P_{in} = 20$ bar) and 2.774 $\times 10^{-3}$ bar ($P_{in} = 10$ bar) for the SA-10-100_A and SA-10-50_B injectors respectively. Additionally, the maximum roughness of the steady state signals, defined here as one standard deviation of the pressure signal at the injector face, are 0.4765 bar and 0.07510 bar for the respective injectors, both measured during $P_{in} = 10$ bar runs. These values show that while pressure coupling is apparent, it is

DOI: 10.13009/EUCASS2019-439

not causing chugging to a significant magnitude. This may be a feature of the injector architecture and will be apparent when the issues with the orifice injectors have been resolved, or it could be related to the thruster scale, where the low mass flow rates and small geometry are less susceptible to chugging that for larger thrusters. Testing this will also require functioning orifice injectors as well as additional Poiseuille injectors with lower fractional pressure drops.

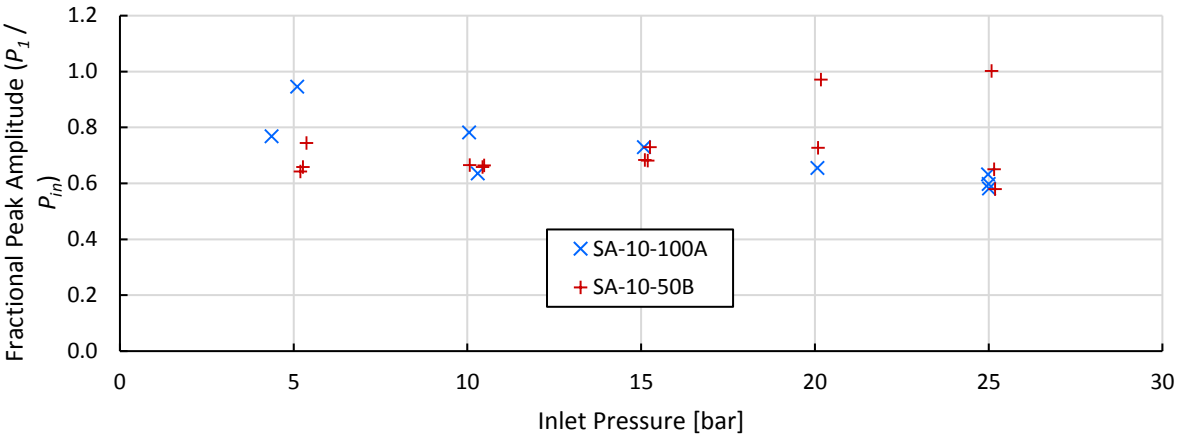

Figure 14: Fractional peak amplitudes of each run, comparing the maximum frequency peaks across the injector ($= P_{1,max}/P_{in,max}$ where P_1 is the injector plane data)

5. Conclusion

This investigation to date has demonstrated some preliminary performance of orifice and Poiseuille injector architectures. The method of injector flow characterisation using DI water has been shown to follow the analytical theory directly for the orifice injector, where $\zeta \propto \dot{m}/\sqrt{dP}$. This is independent of the working fluid, so the geometric parameter here should apply to a flow of HTP or any other propellant. The chemical etching method of manufacturing these orifice injectors appears relatively robust to blockages, which is of concern given the low scales, although the smaller orifices with effective discharge diameters of ~ 0.02 mm did block. Additionally the manufactured geometry needs further characterisation as the contoured orifice walls mean that the discharge diameter is not close to the specified geometry. This wall profiling may also explain the unexpectedly high values for $C_d > 2$, which should be a physical impossibility as $C_d = \dot{m_{exp}}/\dot{m_{ideal}}$. In this case the flow velocity may not be acting as an orifice plate, increasing performance. This is also being investigated further using computational methods and some preliminary results should be presented in this paper after the conference.

The simulation results of the orifice injector exhibit the same trends as the experimental results, albeit with lower values of $C_d < 1$. It is seen that C_d decreases for larger orifices, and while this is not fully understood, it is proposed that this may be due to the increase dominance of viscous forces for larger discharge areas as the working fluid is accelerated less. This may also result in a less pronounced cavitation in the orifice, although this must be demonstrated in computational results. However, the computation model does not yet match the experimental results and ongoing efforts are being made to validate both.

Experimental flow characterisation of Poiseuille injectors has shown good agreement between the Hagen-Poiseuille flow theory and the results, however there are some small nonlinearities in the empirical data. The cause of this is unknown, and it is a current research topic in the microfluidics field, although in the case of these injectors it is proposed that it is due to viscosity or surface tension effects. Further research is required to validate either of these ideas. Despite this, the nonlinearities are small and the performance for a given injector can be determined using the expression $\zeta \propto \dot{m}/dP$.

As with the orifice injector, the simulation results for Poiseuille architectures do not accurately capture the experimental results. The general trends are present, for example C_d decreases with cross-section area, as with orifice injectors, and increases with injector length, however the specific values do not match. The second trend relating C_d with l is currently not understood and needs to be investigated further, although as it is present in the simulation data, it is expected to be a fundamental physical property of Poiseuille injectors.

The preliminary analyses of the coupling of the up and downstream pressures for an injector in a thruster shows some interesting results. Importantly there are pressure-dependant oscillations in the range of 25 Hz to 100 Hz, corresponding to frequencies associated with chugging from literature. While orifice injectors seem to be less robust to blockages and therefore have not been considered, Poiseuille type architectures demonstrate that there is some, albeit reduced coupling between the turbulent frequencies in the bed and the propellant line. The specific causes of these frequencies is at present unknown, as is the effect of Poiseuille injector geometry on the damping effect. It has also

been noticed that the amplitudes of the pressure roughness and these specific oscillatory modes are low, which may suggest that chugging is not such a significant issue for sub-newton scale thrusters, although this needs further work to substantiate. Overall, thruster performance with Poiseuille injectors seems good.

It is important to note that for both of the injector architecture presented, as the respective value for C_d has not been expressed by theory, rather fitted polynomial models, a specific injector must be tested to determine the specific value for ζ to be sure of the specific injector flow characterisation performance. Understanding the parameters that affect C_d is an important next step. It is also clear from ongoing research that the computational model needs further development to capture all of the effects present in the experimental results. Considering turbulence is especially important for the Poiseuille injector architecture as the flow inside the micro-bore tube is likely to a turbulent or transitional regime given the lower onset Reynolds number for microscale flow. This is especially important for understanding how the flow can be decoupled for non-choked injectors, e.g. Poiseuille and potentially porous architectures, although the latter have not been considered in the current work. Further experimental testing is also required to validate any models built to investigate the underlying fluid mechanics.

6. References

[1] D. Krejci and P. Lozano. 2018. Space Propulsion Technology for Small Spacecraft. *Proceedings of the Ieee*. 106,3:362-378.

[2] K. Lemmer. 2017. Propulsion for CubeSats. *Acta Astronautica*. 134,231-243.

[3] F. La Torre, S. Kenjeres, J. L. P. A. Moerel, B. T. C. Zandbergen and C. R. Kleign. 2008. Influence of Boundary Layer Formation and Surface Roughness on the Thrust of Micro-Nozzles. In: *Space Propulsion*. 5th,1-8.

[4] W. F. Louisos, A. A. Alexeenko, D. L. Hitt and A. Zilic. 2008. Design considerations for supersonic micronozzles. *International Journal of Manufacturing Research*. 3,1:80.

[5] G. P. Sutton and O. Biblarz. 2016. Rocket Propulsion Elements.

[6] M. Popp, J. Hulka, V. Yang, M. Habiballah and P. Zarchan. 2004. Liquid Rocket Thrust Chambers. *Progress In Astronautics and Aeronautics*. 200,

[7] J. Hinckel, J. Jorge, T. Soares, M. Zacharias and J. Palandi. 2009. Low Cost Catalysts for Hydrazine Monopropellant Thrusters.

[8] T. R. Nada and A. A. Hashem. 2012. Geometrical characterization and performance optimization of monopropellant thruster injector. *The Egyptian Journal of Remote Sensing and Space Science*. 15,2:161-169.

[9] D. Platt. 2002. A Monopropellant Milli-Newton Thruster System for Attitude Control of Nanosatellites. In: *Small Satellite Conference*.

[10] D. L. Hitt, C. M. Zakrzwski and M. A. Thomas. 2001. MEMS-based satellite micropropulsion via catalyzed hydrogen peroxide decomposition. *Smart Materials & Structures*. 10,6:1163-1175.

[11] E. Fonda-Marsland, C. N. Ryan, G. T. Roberts, A. Lear, E. Fletcher, D. Gibbon and M. Palmer. 2018. Towards Flight Qualification of a 1 Newton Hydrogen Peroxide Thruster. In: *Space Propulsion 2018*. 6th,

[12] J. Huh and S. Kwon. 2017. Microcooling Channel Effect on a Monopropellant Microelectromechanical System Thruster Performance. *Journal of Propulsion and Power*. 33,6:1591-1595.

[13] J. Lee, K. Su-Kyum, S. Kwon and Y. Myoung-Jong. 2012. Fabrication of Catalyst-Insertion-Type Microelectromechanical Systems Monopropellant Thruster. *Journal of Propulsion and Power*. 28,2:396-404.

[14] S. Jo, D. Jang, S. An and S. Kwon. 2011. Chugging Instability of H2O2 Monopropellant Thrusters with Catalyst Reactivity and Support Sizes. *Journal of Propulsion and Power*. 27,4:920-924.

[15] S. Dabiri, W. A. Sirignano and D. D. Joseph. 2007. Cavitation in an orifice flow. *Physics of Fluids*. 19,7:072112.

[16] W. Z. Ai and T. M. Ding. 2010. Orifice plate cavitation mechanism and its influencing factors. *Water Science and Engineering*. 3,3:321-330.

[17] Z. X. Li, D. X. Du and Z. Y. Guo. 2003. Experimental study on flow characteristics of liquid in circular microtubes. *Microscale Thermophysical Engineering*. 7,3:253-265.

[18] D. J. Phares and G. T. Smedley. 2004. A study of laminar flow of polar liquids through circular microtubes. *Physics of Fluids*. 16,5:1267-1272.

[19] D. Brutin and L. Tadrist. 2003. Experimental friction factor of a liquid flow in microtubes. *Physics of Fluids*. 15,3:653-661.

[20] C. H. Choi, K. J. A. Westin and K. S. Breuer. 2003. Apparent slip flows in hydrophilic and hydrophobic microchannels. *Physics of Fluids*. 15,10:2897-2902.

[21] T. Ahmad and I. Hassan. 2010. Experimental Analysis of Microchannel Entrance Length Characteristics Using Microparticle Image Velocimetry. *Journal of Fluids Engineering-Transactions of the Asme*. 132,4:041102.

[22] J. Zhang, S. Yan, D. Yuan, G. Alici, N. T. Nguyen, M. Ebrahimi Warkiani and W. Li. 2016. Fundamentals and applications of inertial microfluidics: a review. *Lab Chip*. 16,1:10-34.

[23] G. R. Wang, F. Yang and W. Zhao. 2014. There can be turbulence in microfluidics at low Reynolds number. *Lab Chip*. 14,8:1452-8.

[24] S. An, J. Jin, J. Lee, S. Jo, D. Park and S. Kwon. 2011. Chugging Instability of H2O2 Monopropellant Thrusters with Reactor Aspect Ratio and Pressures. *Journal of Propulsion and Power*. 27,2:422-427.